Physical Review & Research International
2(2): 75-90, 2012

SCIENCEDOMAIN *international*
www.sciencedomain.org

Phase Evolution in Co-Precipitated Stabilized Zirconia Powders

T. O. Ahmed[1*], P. O. Akusu[1], S. A. Jonah[2] and N. Rabiu[1]

[1]Department of Physics ABU, Zaria, Nigeria.
[2]Centre for Energy Research and Training, ABU, Zaria, Nigeria.

Research Article

Received 28th July 2011
Accepted 7th January 2012
Online Ready 22nd May 2012

ABSTRACT

Zirconia stabilized by addition of bismuth oxide was prepared by co precipitation process from metal oxide chlorides using sodium hydroxide. The dried gels produced pure phase ZrO_2-Bi_2O_3 powders on calcination at 800ºC for the co precipitated powders. The phase evolution was studied and it was found that the delay in obtaining isomorphous ZrO_2-Bi_2O_3 in the co precipitated powders owed to the crystallization of an impure phase BiOCl. This phase was detected in all the calcined co precipitated powders. However, the existence of ZrO_2 as a separate phase was noticed as a common feature. The characterization and structural evaluation of the synthesized powder were carried out by means of Differential Scanning Calorimetry (DSC), Thermogravimetric Analysis (TGA), X-ray Diffraction (XRD), Scanning Electron Microscopy (SEM) and Energy dispersive X- ray Spectroscopy (EDS). Thermal analysis revealed that weight loss arising from evaporation of bound water occurred below 150ºC for all the samples and the sintering temperature was 700ºC. The phase transformation from amorphous ZrO_2 to crystalline ZrO_2 occurred above 600ºC while that from amorphous Bi_2O_3 to crystalline Bi_2O_3 occurred above 700ºC. The crystallite sizes of the synthesized powders were in the range of 8-33nm. SEM micrographs showed a uniform morphology for the calcined powders and revealed nearly spherical powder particles with sizes in the range of 63-101µm. EDS confirmed Zirconia as the major component in all calcined co precipitated powder sample except the sample containing 75.53% Bi.

Keywords: Stabilized zirconia; solid electrolytes; fuel cells; XRD; SEM; EDS.

[*]Corresponding author: Email: tajahmol@yahoo.co.uk;

1. INTRODUCTION

Pure zirconia (ZrO_2) has three crystallographic polymorphs. At room temperature, the stable form of ZrO_2 is the monoclinic mineral baddeleyite. At about 950ºC, it transforms to a tetragonal form, and at 2200ºC, it becomes cubic (Subbarao et al., 1974). Both the tetragonal and cubic forms can be stabilized at room temperature by addition of stabilizers (dopants), which include rare-earth elements or metal oxide impurities ranging from monovalent to trivalent. Though, Yttrium oxide is usually used as the stabilizing component of higher symmetry of zirconia (Zhu, 1998), other stabilizing components are calcium oxide, magnesium oxide, lanthanum oxide and scandium oxide (Subbarao, 1980). Recently, dysprosium oxide was used to stabilize zirconia to produce electrolyte for intermediate-temperature Solid Oxide Fuel Cell (Shankar et al., 2007). Stabilized zirconia has been actively investigated as an oxide ion conductor in Solid Oxide Fuel Cells (SOFCs), oxygen sensors, or electrochemical oxygen pumps (Tanabe et al., 1994; Mamak et al., 2001; Demkov, 2001; Radha et al., 2009). Consequently, several approaches are now being taken to improve the electrical properties of zirconia materials. Structural modification of zirconia is one of promising ways to ameliorate the ionic conductivity of zirconia-based electrolytes (Shankar et al., 2007; Radha et al., 2009; Lei et al., 2005; Santos et al., 2008; Hyun et al., 2007; Bae et al., 2000). Stabilized zirconia solid electrolytes have been found with superior properties at elevated temperatures compared to other ceramic metal oxides like Gd-doped CeO_2, Ba_2InO_2 and (Sr, Mg)-doped $LaGaO_3$ (LSM) when used as electrolytes in solid oxide fuel cells (Subbarao, 1980; Shankar et al., 2007).

It is curious to explore solid electrolyte systems consisting of ZrO_2-Bi_2O_3 because the higher symmetries of the individual oxide system are well- known for enhanced conductivity because of the existence of large concentration of oxygen vacancies in their structures. The possible causes of the conductivity enhancement are (i) the formation of a new kinetic path via a thin interphase layer along the interface between dispersoid and host matrix, (ii) the dispersoid–host interaction leading to an enhanced ionic mobility because of strain effects and (iii) increase in ionic concentration due to space charges either at the interface, around dislocations or due to homogeneous bulk doping (Gupta et al., 2009). Recently, there has been evidence from experiments on the formation of composite solid electrolyte system $[(KCl)_{0.9}:(NaCl)_{0.1}]_{1-y}:(ZrO_2)_y$, indicating enhanced ionic conductivity due to the formation of a new kinetic path via a thin interphase along the interface between dispersoid and halide matrix (Gupta et al., 2009). Sata (2000) and his co-workers reported conductivity enhancement of heterolayered films composed of CaF_2 and BaF_2].

It is a known fact that the dispersion of oxides is not the only way to enhance the conductivity of the solid electrolyte systems. The other techniques also very effective for conductivity enhancement are (i) addition of aliovalent impurities (Yamamoto et al., 1995; Hirano et al., 1999; Hirano et al., 2000; Guangshe et al., 1999), (ii) substitution of host ion with larger ion to open the lattice structure (Lei et al., 2005; Kosacki et al., 2002) and (iii) control on preparative parameters like the applied load for pelletization, sintering temperature and soaking time period, etc. Another report by Azad, (2005) and his co-workers indicated ionic conductivity improvement in gadolinia-doped ceria and zirconia-layered structures compared to individual bulk electrolytes.

More recently, we have demonstrated the possibility of synthesizing nanometer sized stabilized zirconia by incorporating Bi_2O_3 into ZrO_2 matrix using modified co-precipitation method (Ahmed, 2010). The reasons for choosing Bi_2O_3 as the stabilizer are (i) Bi_2O_3 has a high oxide ion conductivity and (ii) Bi^{3+} has lower valence than Zr^{4+}, which promotes the

formation of oxygen vacancies for easy mobility of oxygen ions. Differential Scanning Calorimetry (DSC) and Thermo-Gravimetric Analysis (TGA) show that the sintering temperature in air for the stabilized zirconia is 700ºC. In the entire synthesized samples, there is substantial evidence for the formation of crystalline phases of bismuthoxychloride which are present in minute concentrations at the interface between the host matrix (ZrO_2) and the stabilizer (Bi_2O_3) as confirmed using X-ray Diffractometry and Scanning electron microscopy. The morphology of the synthesized stabilized ZrO_2 as obtained from Scanning electron microscopic analysis confirm that the particles are nearly spherical in shape with little agglomeration and porosity for the entire samples. A follow-up with Energy Dispersive X-ray Spectroscopy reveals the presence of Zr, Bi, Na, O and Cl as the components in all the co precipitated samples.

2. MATERIALS AND METHODS

2.1. Sample Preparation

The samples were prepared using the raw materials zirconium chloride octa-hydrate ($ZrOCl_2.8H_2O$, 99.0% purity, BDH Poole, England), bismuth oxychloride (BiOCl, 99.5% purity, BDH Poole, England) and sodium hydroxide (NaOH, 96%, May & Baker, Nigeria). Others include inorganic and organic reagents: Hydrochloric acid (HCl, assay; 35-37%, Philip Harris, England), distilled water, toluene ($C_6H_5CH_3$, 99.7%, BDH Poole, England), propanol ($[CH_3]_2CHOH$, 99.7%, BDH Poole, England), ammonia solution (NH_3, assay; 33%, Griffin & George) and filter paper (12.5cm Grade, Whatman, England).

Using the materials mentioned above, the concentration of Zirconylchloride and Bismuthoxychloride solutions used are 1M in acidic medium (50% HCl), with 100ml 3M NaOH as neutralizer. The homogeneous mixture of $ZrOCl_2.8H_2O$ and BiOCl powders in different mol% ($x = 0.08, 0.12, 0.18, 0.40, 0.50$) was made at room temperature. The precipitation bath was carried out with 3M-NaOH and the mixture was filtered, washed and dried at 200ºC in an oven for 2h. The samples were then sintered in air at 800ºC for 4 h to yield the nano-sized particles. The calcined powder is mixed with polyvinyl chloride (PVC) and toluene as binder and cold pressed into cylindrical pellets of 25 mm diameter and 2 mm thickness using a hydraulic press at 16kPa uniaxial pressure. These pellets are then sintered at 800ºC for 4 h in air and dense crack-free pellets are obtained from these powders. After cooling to ambient temperature, the samples became pale yellow.

2.2. Experimental Techniques

The solid solutions $(ZrO_2)_{1-x}$ $(Bi_2O_3)_x$ were characterized by XRD to detect the possibility of any new phase(s) formation during synthesis. The X-ray diffraction (XRD) patterns at room temperature were recorded by X-ray Diffractometer Diffrac Bruker AXS, D8 Advanced Plus, at 30 mA and 35 kV, with monochromatic CuK_α radiation, of wavelength λ= 1.5450Å. A scanned range 15–80º 2θ, with a step width of 0.02º was used. The sample was also subjected to thermal analyses (DSC and TGA) using an automatic micro thermal analyzer (Netzsch STA 449 Thermal analysis instrument) for further confirmation of any chemical compound formation. The thermal analyses were carried out in the temperature range of ambient to 800ºC with a scanning rate of 10ºC/min.

In order to study the microstructure of the samples and to examine the formation of interface between the host matrix and the stabilizer, micro structural investigation of $(ZrO_2)_{1-x}$:$(Bi_2O_3)_x$

samples was done using a scanning electron microscope (SEM) Leica- Cambridge, Stereoscan 440. An Energy Dispersive X-ray Spectroscope EDS, Oxford ISIS, microanalyser integrated equipped with SEM was used to delineate the elemental composition of the solid solutions.

3. RESULTS AND DISCUSSION

3.1. Scanning Electron Microscopy

The microstructural investigations of the co precipitated powders in the system $(ZrO_2)_{1-x}:(Bi_2O_3)_x$ were carried out and the micrographs for the compositions A,B,C are presented in Fig. 1 which shows that the grains are interspersed with the ZrO_2 particles. The development of interfaces can also be predicted qualitatively from the micrograph (Fig. 1). However, the existence of ZrO_2 as a separate phase was noticed as a common feature. The mixed oxide grains can also be contrasted as the Bi_2O_3 appearing as dark grain is overlaid by much clustered ZrO_2 in lighter contrast. The contrast observed in the mixed oxide phase arises from two principal sources: first, the lightness of the zirconia phase compared with darker bismuth oxide background is mostly due to the difference in secondary electron yield of the two phases. Zirconia being less conducting has much the higher yield. The second cause of contrast is topographical, arising from the angular variations that the zirconia phase makes with the incident beam. In Figs. 1(A) and 1(B), the particles are nearly spherical in shape and the distribution of the particles is such that they are closely packed together.

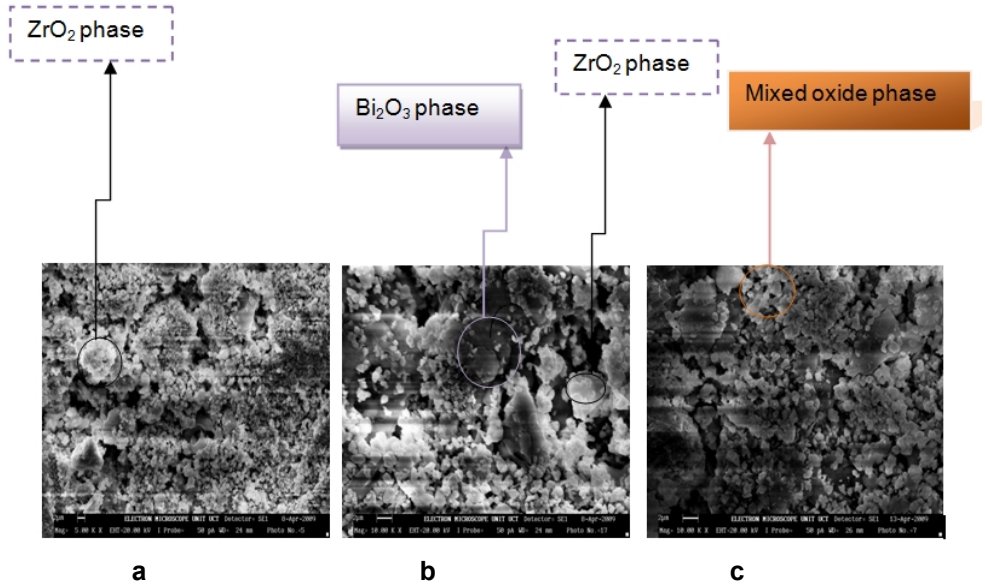

Fig. 1. The SEM Micrograph for co-precipitated samples: (a) $(ZrO_2)_{0.92}(Bi_2O_3)_{0.08}$, (b) $(ZrO_2)_{0.88}(Bi_2O_3)_{0.12}$ and (c) $(ZrO_2)_{0.82}(Bi_2O_3)_{0.18}$

The average particle size is determined from SEM with imaging software (Image-J) to be 101±4μm and 94±4μm respectively. The microstructure for sample C (Fig.1C) shows clear boundary between the agglomerated grains of the mixed oxide phase with ZrO_2 particles

interspersed on the surface of the grains and along the grain boundaries. The average particle size is determined from SEM with imaging software (Image-J) to be 63±3μm.

The microstructure for co-precipitated samples in Figs. 2(a) and 2(b), is quite different from that of the previously discussed solid electrolytes [Figs.1(a)-(c)]. The development of interfaces can also be predicted qualitatively from the micrograph (Fig. 2). However, the existence of ZrO_2 as a separate phase was noticed as a common feature but the mixed oxide phase appears much more agglomerated with plate like formation. Qualitatively, the ZrO_2 phase is interspersed on the platy grains of the mixed oxide and along the interfaces. The average particle size is determined from SEM with imaging software (Image-J) to be 75±4μm and 67±2μm respectively. In conclusion, the morphology of the synthesized solid electrolytes revealed that the particles are nearly spherical in shape and with little agglomeration for samples shown Figs 1 (a)-(c) while for samples in Figs. 2(a) and (b) there is much more agglomeration leading to plate-like formation. The average particle size decreases with increase in volumetric concentration of dopant (Bi_2O_3) with a broad particle size distribution.

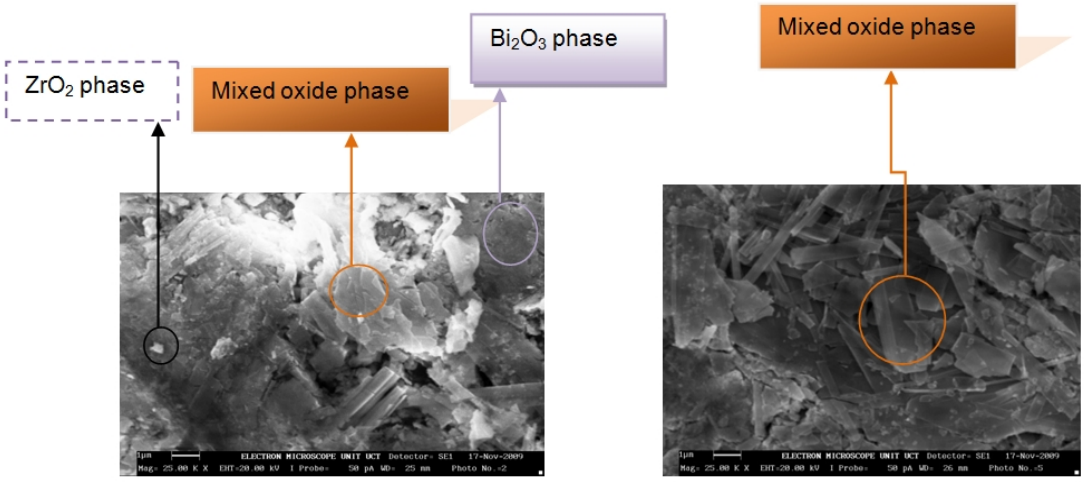

d **e**

Fig. 2. The SEM Micrograph of Solid Electrolyte samples: (a) $(ZrO_2)_{0.6}(Bi_2O_3)_{0.4}$ and (b) $(ZrO_2)_{0.5}(Bi_2O_3)_{0.5}$

3.2. EDS Analyses

The X-ray microanalysis confirmed the presence of zirconium, bismuth, oxygen, sodium and chlorine as the components of the co-precipitated powder samples. Zirconium and bismuth were detected with higher relative concentrations compared to the other components. The quantitative analytic results for the co-precipitated powder samples are presented in Table 1. Figs. 3 (a)-(e) show the EDS spectra of the co-precipitated powder samples. It can be found that the peak intensity of the Zr-L_α is much stronger than the peak intensity of Bi-M_α for all the samples. Qualitatively, the peak intensities of Cl-K_α and Na-K_α are more enhanced compared with that of O-K_α, with shorter live time.

Table 1. Concentration of various elements in the stabilized zirconia solid solutions

Sample	Element	Line	Wt.%	Error	K-ratio	Atomic%
	O	$K_{\sim}$	1.22	0.034	0.0100	5.28
	Na	$K_{\sim}$	1.94	0.029	0.029	5.85
a	**Cl**	$K_{\sim}$	18.34	0.149	0.2130	35.85
	Zr	$L_{\sim}$	63.08	0.341	0.6117	47.91
	Bi	$M_{\sim}$	15.42	0.189	0.1050	5.11
	O	$K_{\sim}$	5.41	0.199	0.0427	17.48
	Na	$K_{\sim}$	6.10	0.143	0.0642	13.71
b	**Cl**	$K_{\sim}$	18.03	0.393	0.1982	27.21
	Zr	$L_{\sim}$	57.19	0.930	0.5111	32.39
	Bi	$M_{\sim}$	13.27	0.296	0.1144	9.21
	O	$K_{\sim}$	1.15	0.029	0.0094	4.98
	Na	$K_{\sim}$	1.66	0.024	0.0184	5.02
c	Cl	$K_{\sim}$	18.88	0.136	0.2191	36.94
	Zr	$L_{\sim}$	63.16	0.305	0.6122	48.03
	Bi	$M_{\sim}$	15.15	0.168	0.1032	5.03
	O	$K_{\sim}$	-	-	-	-
	Na	$K_{\sim}$	-	-	-	-
d	Cl	$K_{\sim}$	30.69	0.232	0.3636	45.07
	Zr	$L_{\sim}$	40.28	0.328	0.3955	45.31
	Bi	$M_{\sim}$	29.03	0.328	0.2035	9.61
	O	$K_{\sim}$	0.07	0.004	0.0008	0.51
	Na	$K_{\sim}$	-	-	-	-
e	Cl	$K_{\sim}$	11.41	0.056	0.1633	38.77
	Zr	$L_{\sim}$	13.00	0.074	0.1529	17.17
	Bi	$M_{\sim}$	75.53	0.197	0.6506	43.55

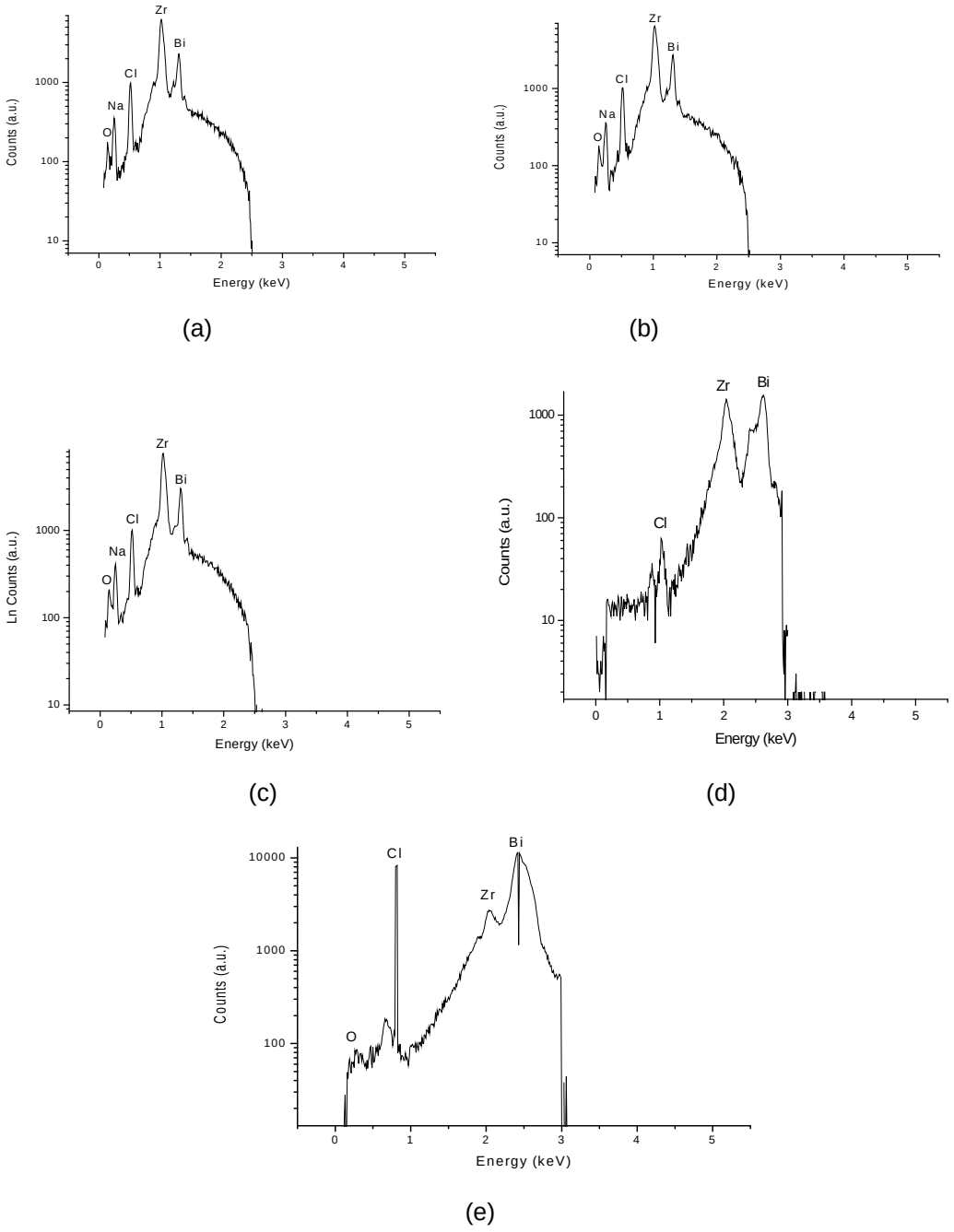

Fig. 3. EDS Spectra for co-precipitated samples: (a) $(ZrO_2)_{0.92}(Bi_2O_3)_{0.08}$, (b) $(ZrO_2)_{0.88}(Bi_2O_3)_{0.12}$, (c) $(ZrO_2)_{0.82}(Bi_2O_3)_{0.18}$, (d) $(ZrO_2)_{0.6}(Bi_2O_3)_{0.4}$ and (e) $(ZrO_2)_{0.5}(Bi_2O_3)_{0.5}$

Even with much shorter live time, the peak of O-K_α in the co-precipitated powder samples is also discerned clearly. Qualitatively, under the same accelerating voltage, the relative concentration of O depreciated to 0.06% as the dopant concentration increases. The chlorine content ranges from 11.41% to 30.69%. The chlorine content in the co-precipitated powders can be associated to the presence of NaCl, $BiCl_3$, BiOCl and $ZrCl_4$. Furthermore, the microanalysis of the co-precipitated powder sample (d) indicates 30.69% of Cl content, which may only be due to any chloride form of zirconium and bismuth as the chlorides of ammonium and sodium are not stable at high temperatures.

This suggests that the co-precipitated powder has a significant amount of entrapped unreacted chlorides of zirconium and bismuth during precipitation process. The same reason could also be extended to the entrapment of NaCl in the precipitates for co-precipitated powder samples (a)-(c) as chlorine content is significantly high. In contrast, the microanalysis of the co-precipitated powder samples (d) and (e) did not indicate the presence of sodium; this elimination may be due to excessive washing with doubly distilled water as it is easier to get rid of sodium compared to chlorine. The reduction in chlorine content in the co-precipitated powder sample (e) might be owed to the fact that greater percentage of bismuth chloride is converted to its oxide as compared to that of zirconium. The same logic could also be extended to the conversion of chloride of zirconium in preference to that of bismuth in the other co-precipitated powder samples.

3.3. Thermal Analysis

The combined DSC-TGA curves in Figs. 4 (a)-(c) represent the decomposition behavior of the individual metal hydroxides. It can be seen that the decomposition of $Zr(OH)_4$ takes place in two stages (blue curves Figs. 4a-c). The endothermic peak at 130ºC represents the loss of adsorbed moisture in the co-precipitated powders. The peak at 210ºC may be assigned to the volatilization of ammonia and n-propanol used during washing from the system. The subsequent endothermic peak at 260ºC and the broad endothermic peak in the range 500ºC-600ºC correspond to the decomposition of $Bi(OH)_3$ and $Zr(OH)_4$ to their amorphous oxide states respectively. This is accompanied by considerable weight losses of 64.04%, 68.66% and 48.79% (black curves) which are complemented by the associated exothermic peaks at 100ºC and 250ºC for samples (a), (b) and (c). The onset of transformation into a stable monoclinic ZrO_2 phase is observed above 600^{o}C up to a saturation temperature of 700ºC. This is evident from the powder pattern for the samples (Figs. 5a-c) and conforms with the work of Santos (2008) and coworkers; where the transformation to monoclinic ZrO_2 phase was observed above 600ºC. The results indicate that the calcination temperature for the precipitated samples is 700ºC and this corresponds to 49.38%, 60.57% and 73.61% losses in weight at 800ºC. The results presented in Figs. 4(a)-(c) are in good agreement with the work led by Shankar, (2007) in which the saturation (sintering) temperature was observed at 700ºC.

Fig. 5(a) shows exothermic peaks at 100ºC and 200ºC while endothermic peaks at 130ºC and 220ºC. Following these transformations is a considerable weight loss of 46.28% due to evaporation of moisture content. Transformation into tetragonal phase of ZrO_2 occurs above 600ºC while the cubic Bi_2O_3 phase occurs above 700ºC, but this is accompanied by a tetragonal Bi_2O_3 phase. This deduction is in accordance with the phase transformation of low symmetry phase of Bi_2O_3 to higher symmetry phase above 727ºC, which on cooling leads to possible formation of tetragonal and body centered cubic phases. The overall weight loss of 71.83% was observed at saturation temperature.

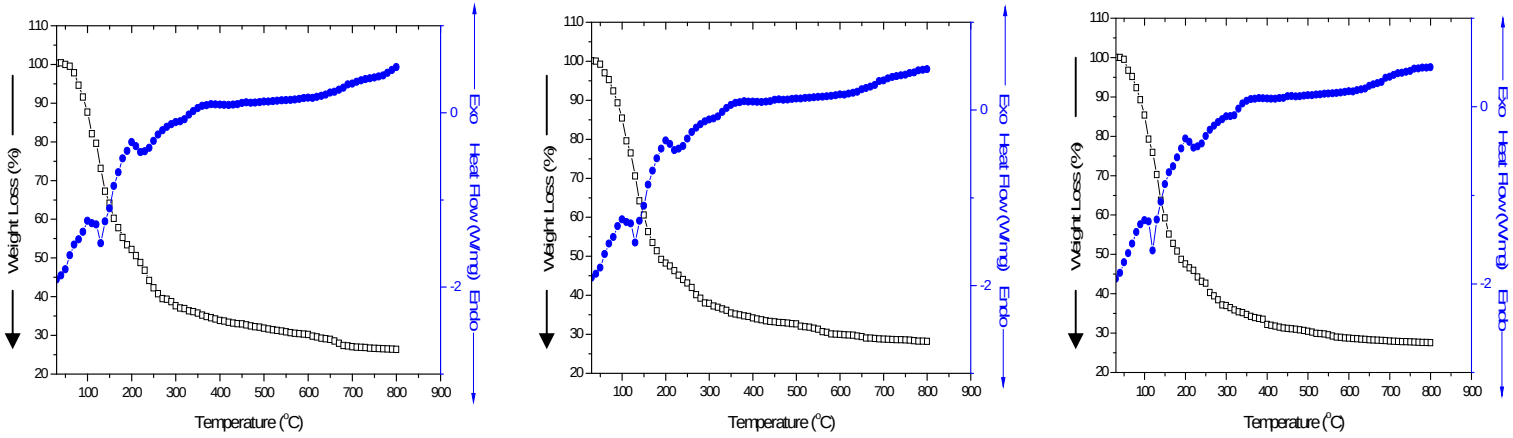

Fig. 4. DSC-TGA for co-precipitated samples: (a) $(ZrO_2)_{0.92}(Bi_2O_3)_{0.08}$, (b) $(ZrO_2)_{0.88}(Bi_2O_3)_{0.12}$ and (c) $(ZrO_2)_{0.82}(Bi_2O_3)_{0.18}$

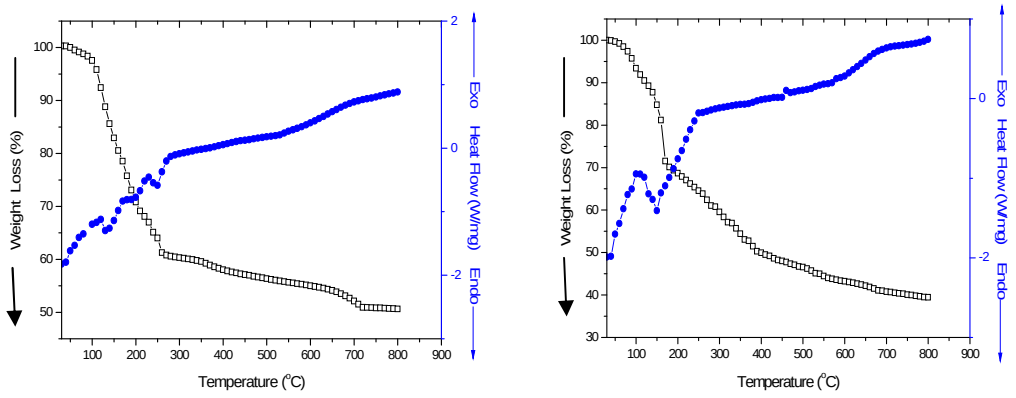

Fig. 5. DSC-TGA for (a) $(ZrO_2)_{0.6}(Bi_2O_3)_{0.4}$ and (b) $(ZrO_2)_{0.5}(Bi_2O_3)_{0.5}$

In Fig. 5(b), the peaks at 100ºC and 200ºC are associated with exothermic transformations while those at 120ºC and 220ºC are associated with endothermic transformations (blue curve). The effect of these transformations corresponds to a weight loss of 45.89%. Phase transformations into monoclinic Bi_2O_3 and orthorhombic ZrO_2 phases occur at 330ºC while the cubic Bi_2O_3 phase occurs above 700ºC. A constant weight loss above the transformation temperature up to a saturation point is followed by an overall weight loss of 72.46%.

The thermo-gravimetric analysis (TGA) of the co-precipitated powders is in agreement with the DSC peaks showing distinct regimes of weight loss corresponding to the temperature regions mentioned in the DSC. The TGA of the co-precipitated powders shows a weight loss of more than 50% and most of it occurs below 500ºC with a slight weight loss continuing up to 700ºC. This large weight loss could be because of the dehydroxylation of hydroxides, conversion of metal chlorides into oxides as well as removal of excess NaCl from the system. In the temperature range 700ºC -800ºC, there is no significant weight loss reflecting that the saturation temperature for the co-precipitated powders is 700ºC. This deduction fits well with the results of elemental analysis and XRD analysis.

3.4. XRD Analyses

X-ray diffraction analyses of the co-precipitated powder samples were carried out and the patterns are given in Fig. 6(a)-(c) and Fig. 7(a) and (b). The intense peaks in the XRD patterns of the co-precipitated powder samples lie in the angular (2θ) range of 15º and 80º. The patterns were analysed and the peaks were identified using ICDD data file. It can be seen from the Fig6(a)-(c), that besides a very few minor peaks of bismuth oxychloride with low intensity, majority of the peaks belong to ZrO_2, indicating that the lattice structure of the mixed oxide matrix is primarily of ZrO_2 type. The XRD patterns of the co-precipitated powder samples in Fig. 6 (a) and (c) indicates that the intensity of the peaks (111) and (-111) is being modulated because of the presence of Bi_2O_3 in the ZrO_2 unit cell. This shows that the some of the dopant atoms occupy similar positions as the host atoms thereby leading to the dopant adopting the structure of the host matrix. The cause of lower intensity of the dopant phase may be attributed to its lower proportion (mole fraction) in the co-precipitated powder samples as compared to host matrix. X-ray diffraction patterns of the as-synthesized co-

precipitated powders (Fig.6 a-c) showed sharply defined peaks of BiOCl (JCPDS File card no. 6-0249) indicating its presence in a significant amount. In particular there are no peaks for any compounds, including chlorides and hydroxides of zirconium and sodium found in the co-precipitated powders. The diffractogram indicates that all such compounds may be present in the powders in an amorphous form.

The co-precipitated powders calcined at 800ºC for 4 h showed crystallization peaks of BiOCl (JCPDS File card no. 6-0249) (Swansonr et al., 1955). However, crystallization peaks of ZrO_2 of monoclinic symmetry could be observed for co-precipitated powders calcined at 800ºC for 4 h, and the maximum peak in the diffractogram corresponded to the maximum peak position of crystalline ZrO_2 (ICDD File card no. 01-083-0937) (Ahmed, 2010). The unit cell parameters for the monoclinic ZrO_2 were obtained from Rietveld least square refinement to be $a = 5.0792$ Å, $b = 5.2290$ Å and $c = 5.3385$ Å for co-precipitated powder sample (a), $a = 5.1734$ Å, $b = 5.2041$ Å and $c = 5.3420$ Å for co-precipitated powder sample (b) and $a = 5.1608$ Å, $b = 5.2288$ Å and $c = 5.3442$ Å for co-precipitated powder sample (c). The variation in the unit cell dimension is due to unit cell expansion due to incorporation of dopant with uncertainty in all cases less than 1%. The unit cell of BiOCl is tetragonal and the XRD peak positions varied slightly for the co-precipitated powder samples corresponding to variations in cell dimensions within the limits $a = 3.81 - 3.83$ Å, $c = 7.52 - 7.54$ c = 7.52-7.54 Å and $c/a = 1.96 - 1.97$. The crystallite sizes of the co-precipitated powders were calculated from the peak broadening of X-ray diffractograms using Scherrer equation. The crystallite sizes were 29nm, 26nm and 21nm respectively for the co-precipitated powders calcined at 800ºC.

The XRD patterns for the as-synthesized co-precipitated powder samples containing higher concentration of dopant shown in Fig. 7 (a) and (b) are quite different from those shown in Fig 6(a)- (c). In the co-precipitated powders, there is ample amount of chloride; so amorphous Bi_2O_3 may have reacted with chloride to form the BiOCl phase as per the following equation:

$$Bi_2O_3 + BiCl_3 \rightarrow 3BiOCl \quad (1)$$

The presence of BiOCl peaks in XRD pattern (Fig. 7a) suggests that BiOCl is a very stable chloride in comparison with Na chlorides, and this may have delayed the formation of ZrO2 and Bi_2O_3 phases. The decrease in intensity of BiOCl peaks in the diffractograms indicates the gradual disappearance of that phase. This may have occurred as per the following reaction:

$$4BiOCl + O_2 \rightarrow Bi_2O_3 + 2Cl_2 \quad (2)$$

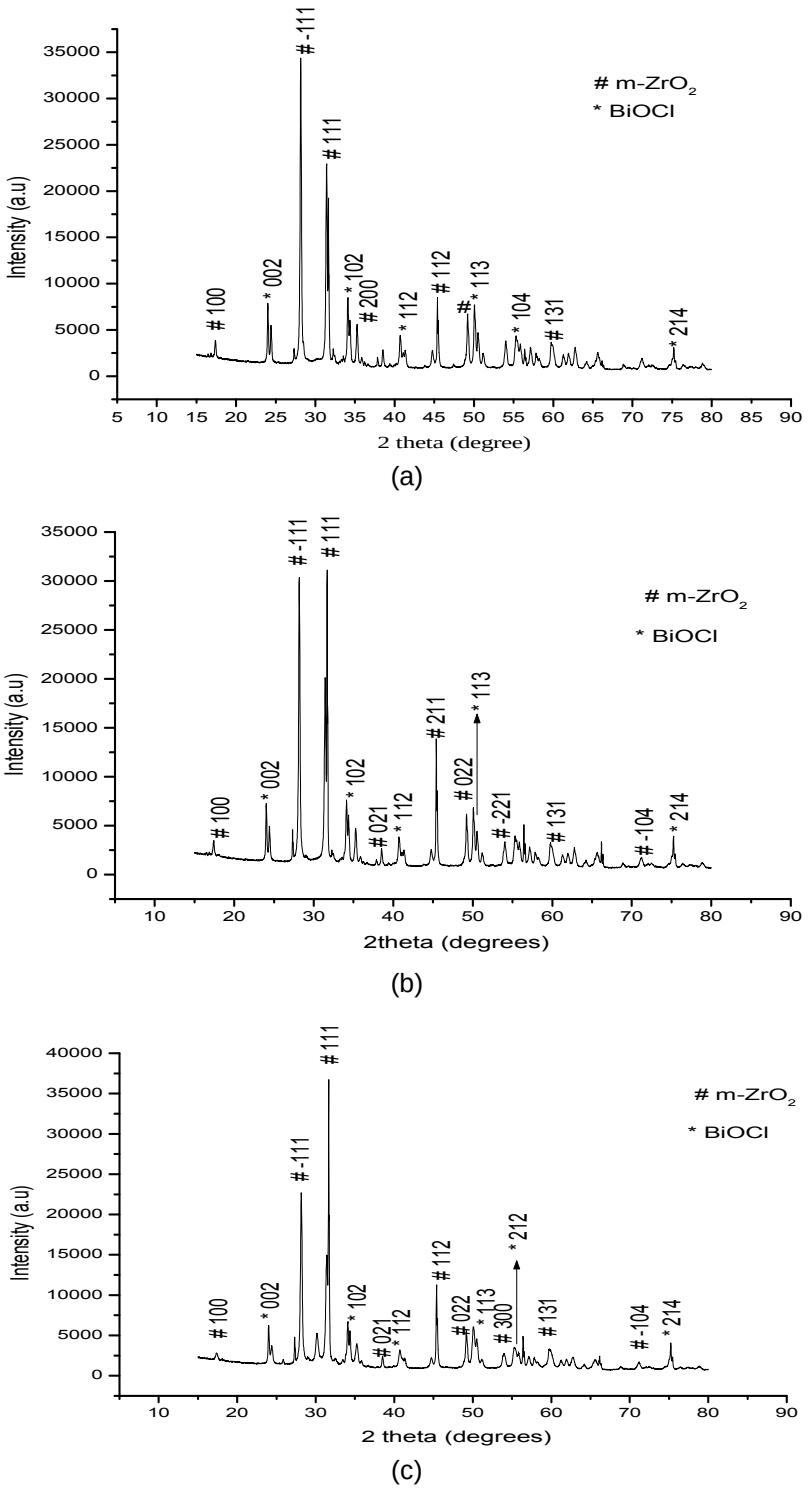

Fig. 6. XRD patterns for co-precipitated samples: (a) $(ZrO_2)_{0.92}(Bi_2O_3)_{0.08}$, (b) $(ZrO_2)_{0.88}(Bi_2O_3)_{0.12}$ and (c) $(ZrO_2)_{0.82}(Bi_2O_3)_{0.18}$

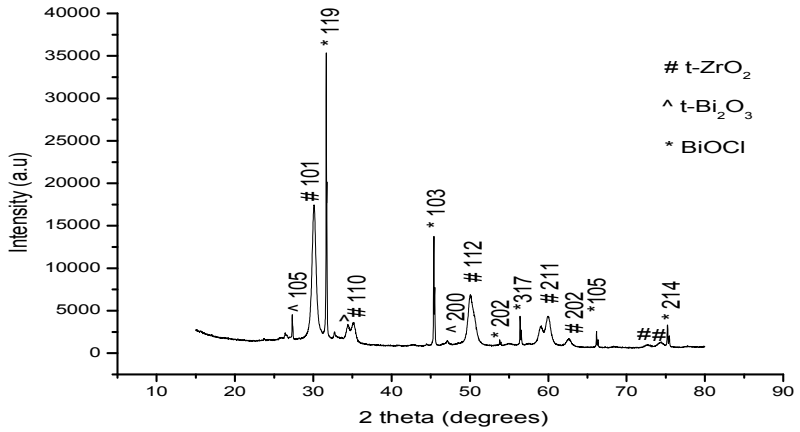

(a)

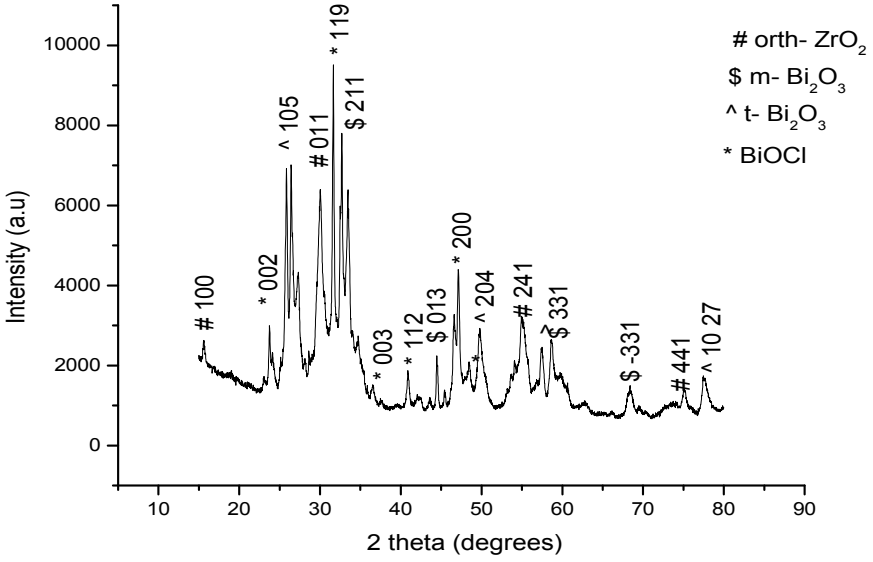

(b)

Fig. 7. XRD Patterns for co-precipitated samples (a) $(ZrO_2)_{0.6}(Bi_2O_3)_{0.4}$ and (b) $(ZrO_2)_{0.5}(Bi_2O_3)_{0.5}$

Though the system takes oxygen from the atmosphere, there is also a loss of 2 mol of chlorine for every mole of oxygen coming into the system. This is well supported by a small and continued weight loss at higher temperatures in the TGA curve (Fig. 5a). The unit cell parameters of tetragonal ZrO_2 were calculated to be $a = 3.6177$ Å, $c = 5.6500$ Å and $c/a = 1.5618$ while that for tetragonal BiOCl ($a = 3.84 - 3.85$ Å, $c = 7.53 - 7.54$ Å and $c/a = 1.95 - 1.96$) (Swansonr et al., 1955). The crystallite sizes were 8nm, 15nm and 33nm respectively for the different phases present in the co-precipitated powders calcined at 800ºC.

Finally, the XRD pattern for the co-precipitated powder sample shown in Fig. 7(b) is very complicated. The presence of chlorine in the system as BiOCl might have reacted with the amorphous Bi_2O_3 to form this phase. However, crystallization peaks of Bi_2O_3 of monoclinic and tetragonal symmetries could be observed for co-precipitated powders calcined at 800^oC for 4 h, and the maximum peak in the diffractogram corresponded to the maximum peak position of crystalline tetragonal Bi_2O_3 (ICDD File card no. 01-076-2477) (Ahmed, 2010). The presence of BiOCl peaks in XRD pattern (Fig. 7b) suggests that bismuthoxychloride is a very stable chloride in comparison with sodium chlorides, and this may have delayed the formation of ZrO_2 and Bi_2O_3 phases. The decrease in intensity of chlorides of bismuth peaks in the diffractograms indicates the gradual disappearance of that phase and this is in accordance with the above equation (2) and the fact that the percentage weight of chlorine (11.41%) is small compared with that in the co-precipitated sample (d). This is well supported by the small percentage of chlorine in comparison with other samples in the EDS analysis (Table 1).

The unit cell parameters of orthorhombic ZrO_2 were calculated to be $a = 3.6177$Å, $b = 6.5216$ Å and $c = 7.5121$Å while that for tetragonal BiOCl is $a = 3.85$Å, $c = 7.52$Å and $c/a = 1.95$. For the tetragonal Bi_2O_3 phase $a = 3.6640$ Å and $c = 20.7269$Å while that for the monoclinic Bi_2O_3 phase is $a = 5.9596$ Å, $b = 8.1644$ Å and $c = 7.5121$Å. The crystallite sizes were 9nm, 15nm, 12nm and 14nm respectively for the different phases present in the co-precipitated powders calcined at 800^oC.

4. CONCLUSION

A wet chemical method has been employed for the synthesis of co precipitated stabilized zirconia powders in nano scale with high sinter ability. The thermal analyses (DSC-TGA) revealed the sintering temperature for the co precipitated stabilized zirconia to be 700ºC, which is owed to the constant weight losses between 700ºC-800ºC for all the samples. This analysis revealed that weight loss arising from evaporation of bound water occurred below 200ºC for all the samples. The phase transformation from amorphous Zirconia to monoclinic began above 600ºC and that from amorphous Bi_2O_3 occurred above 700ºC. Analysis of the X-ray diffraction patterns of the stabilized zirconia powders revealed the presence of crystalline BiOCl phase, which is attributable to the fact that bismuthoxychloride is a very stable chloride in comparison with sodium chlorides, and this may have delayed the formation of ZrO_2 and Bi_2O_3 phases. The crystallite sizes of the phases present in the co precipitated powders are in the range of 8-33nm. The morphology of the synthesized powder as obtained from SEM analysis revealed that the particles are nearly spherical in shape and had broad particle size distribution with little agglomeration and porosity. The particle size increases with increase volumetric concentration of dopant with values ranging from 63-101µm. Finally, EDS analysis confirmed the presence of Zirconium, bismuth, chlorine, sodium and oxygen as the components of the co precipitated powders with zirconium having higher concentration in all the samples except the sample with 75.53% Bi.

ACKNOWLEDGMENTS

We thank the University Board of Research (Ahmadu Bello University, Zaria, Nigeria) for the financial support during the research work and iThemba Labs and Electron microscope unit (University of Cape town, South Africa) for technical assistance during the experimental characterization.

COMPETING INTERESTS

Authors have declared that no competing interests exist.

REFERENCES

Ahmed, T.O. (2010). Synthesis and structural evaluation of $(ZrO_2)_{1-x}(Bi_2O_3)_x$ solid electrolytes. Unpublished PhD dissertation, department of physics, Ahmadu Bello University, Zaria, Nigeria.

Azad, S., Marina, O.A., Wang, C.M., Saraf, L., Shutthanandan, V., McCready, D.E., El-Azab, A., Jaffe, J.E., Engelhard, M.H., Peden. C.H.F., Thevuthasan, S. (2005). Appl. Phys. Lett., 86, 131906–131911.

Bae, J.W., Park, J.Y., Hwang, S.W., Yeom, G.Y., Kim, K.D., Cho, Y.A., Jeon, J.S., Choi, D. (2000). Characterization of yttria- stabilized zirconia thin films prepared by radio frequency magnetron sputtering for a combustion control oxygen sensor. J. Electrochem. Soc., 147(6), 2380-2384.

Demkov, A.A. (2001). Investigating alternative gate dielectrics: a theoretical approach. phys. Status Solidi B, 226(1), 57- 67.

Guangshe, L., Feng, L.S., Wang, M., Zhang, L., Yao, X. (1999). An effective synthetic route for a novel electrolyte: nanocrystalline solutions of $(CeO_2)_{1-X}(BiO_{1.5})_X$. Adv. Mate., 11(2).

Gupta, A., Sil, A., Verma, N.K. (2009). Preparation, characterization and ionic conductivity studies of ZrO2 dispersed mixed halide matrix (KCl)0.9-(NaCl)0.1. Journal of Physics & Chemistry of Solids, 70(2), 340-343.

Hirano, S., Watanabe, S., Kato, E., Mizutani, Y., Kawai, M., Nakumura, Y. (1999). High electrical conductivity and high fracture strength of Sc_2O_3-doped zirconia ceramics with submicrometer grains. J. Am. Ceram. Soc., 82(10), 2861-2864.

Hirano, M., Inagaki, M., Mizutani, Y., Nomura, K., Kawai, M., Nakumura, Y. (2000). Improvement of mechanical and electrical properties of scandia-doped zirconia ceramics by post-sintering with hot isostatic pressing. J. Am. Ceram. Soc., 83(10), 2619-2621.

Hyun, J.Y., Cho, K.H., Mo, I.J., Shim, D.W. (2007). Fabrication of yttria stabilized zirconia films as the electrolyte of micro-fuel cells by Aerosol Flame Deposition. Journal of Ceramic Process Research, 8(3), 213-218.

Kosacki, I., Anderson, H.U. (2002). Nonstoichiometry & electrical transport in scandia- doped zirconia solid state ionics. 152- 53, 431- 438.

Lei, Z., Zhu, Q. (2005). Low temperature processing of dense nano-crystalline scandia doped zirconia (ScSZ) ceramics. Solid State Ionics.

Mamak, M., Coombs, N., Ozin, G.A. (2001). Electro active mesoporous yttria stabilized zirconia containing platinum or nickel oxide nanoclusters: a new class of solid oxide fuel cell electrode materials. Adv. Funct. Mater., 11(1), 59-63.

Radha, A.V., Oscar, B.M., Sergey, V.U., Alexandra, N., Pedro, T. (2009). Surface enthalpy, enthalpy of water adsorption and phase stability in nanocrystalline monoclinic zirconia. J. Am. Ceram. Soc., 92(1), 133-140.

Santos, V., Zeni, M., Bergmann, C.P., Hohemberger, J.M. (2008). Correlation between thermal treatment and tetragonal/monoclinic nanostructured zirconia powder obtained by sol-gel process. Rev. Adv. Mater. Sci., 17, 62-70.

Sata, N., Eberman, K., Eberl, K., Maier, J. (2000). Mesoscopic fast ion conduction in nanometer-scale planar heterostructures. Nature, 408, 946-949.

Shankar, S.R., Jayakanth, R., Maiti, S., Kumar, A., Manna, I. (2007). Synthesis and characterization of nanocrystalline dysprosia stabilized zirconia for intermediate-temperature solid oxide fuel cells. Materials Science Eng. B, 1-14.

Subbarao, E.C., Miati, H.S., Srivastava, K.K. (1974). Martensitic transformation in Zirconia. Phys Solidi, 21(1), 9-40.

Subbarao, E.C. (1980). Solid electrolytes and their applications. Plenum Press, New York, 1-17.

Swansonr, H.E.,. Fuyat, K., Ugrinic, G.M. (1955). Natl. Bur. Stand. (U.S.) Circ., 539(4), 54, (JCPDS File Card. No. 6-0249).

Tanabe, K., Yamaguchi, T. (1994). Acid-base bifunctional catalysis by zro_2 and its mixed oxides. Catal. Today, 20(2), 185- 189.

Yamamoto, O., Arati, Y., Takeda, Y. (1995). Electrical Conductivity of Zirconia stabilized with Ytterbia & Scandia Solid State Ionics, 79, 137-142.

Zhu, W.Z. (1998). Effect of cubic phase on the kinetics of the isothermal tetragonal to monoclinic transformation in ZrO_2(3mol%Y_2O_3) ceramics. Ceramics International, 24, 35-43.

© 2012 Ahmed et al.; This is an Open Access article distributed under the terms of the Creative Commons Attribution License (http://creativecommons.org/licenses/by/3.0), which permits unrestricted use, distribution, and reproduction in any medium, provided the original work is properly cited.